Electronic Supplementary Material (ESI) for Nanoscale.

Supporting Information

Pathway-dependent gold nanoparticle formation by biocatalytic self-assembly

Jugal Kishore Sahoo[a, b], Sangita Roy[a], Nadeem Javid[a, c], Krystyna Duncan[a], Lynsey Aitken[a], and Rein V. Ulijn[d, e. f]*

[a]*westCHEM, Department of Pure and Applied Chemistry, Technology and Innovation Center, University of Strathclyde, Glasgow, G1 1RD, UK*

[b]*Current Address: Department of Chemical and Biomolecular Engineering, McCourtney Hall, University of Notre Dame, IN, 46556, USA.*

[c]*School of Chemistry and Biosciences, University of Bradford, UK.*

[d.]*Advanced Science Research Center at the Graduate Center of the City University of New York, 85 Saint Nicholas Terrace, New York, NY 10031, USA.*
[e]*Ph.D. programs in Biochemistry, Chemistry and Physics. The Graduate Center of the City University of New York, NY 10016, USA.*

[f]*Department of Chemistry, Hunter College, City University of New York, 695 Park Avenue, New York, NY 10065, USA*

Materials and Methods

Materials:

All commercial reagents were used as purchased. All solvents were used as supplied (analytical or HPLC grade) without further purification. All chemical reactions were performed in oven-dried glassware and magnetically stirred. Thin layer chromatography (TLC) was performed on Merck silica gel 60 F254 plates. All compounds were visualized either by UV light source (254 nm) or by dipping in basic permanganate solution. Column chromatography was carried out by using silica gel 60 (230-400 mesh). ^{1}H and ^{13}C nuclear magnetic resonance (NMR) spectra were recorded on Bruker AV300 spectrometer in the deuterated solvents. All chemical shifts (δ) are quoted in ppm and coupling constants (J) given in Hz. Residual signals from the solvents were used as an internal reference.

Instrumentation

UV-visible absorption spectroscopy

UV-Vis absorption spectra were recorded in Jasco V-660 spectrophotometer. Samples for the measurement were prepared in PMMA cuvettes (Fisher Scientific).

Fluorescence emission spectroscopy

Fluorescence emission spectra were measured on a Jasco FP-6500 spectrofluorometer with light measured orthogonally to the excitation light, at a scanning speed of 200 nm min^{-1}. The excitation wavelength was 343 nm and emission data were recorded in the range between 360 and 700 nm. The spectra were measured with a bandwidth of 3 nm (or 5 nm) with a low (or medium) response and a 1 nm data pitch. Samples were prepared in PMMA cuvettes (Fisher Scientific) and the time-dependent spectra were recorded immediately.

Circular dichroism (CD)

Circular dichroism (CD) spectra were measured on a Jasco J600 spectropolarimeter in a 0.1 mm path length cylindrical cell, with 1 s integration, step resolution of 1 mm, response of 0.5 s with a bandwidth of 1 nm and slit width of 1 mm. The freshly prepared samples were directly added to the cell (200 µL) using a pipette and the

spectra were recorded after 24 h. The High Tension (HT) voltage value reaches maximum below 225 nm and CD couldn't be measured.

High performance liquid chromatography (HPLC)

Dionex P680 HPLC system was used to quantify the percentage conversion of the enzymatic reaction. A 50 μL sample was injected onto a Macherey–Nagel C18 column of 250 mm length with an internal diameter of 4.6 mm and 5 mm fused silica particles at a flow rate of 1 mL min-1 (eluting solvent system: linear gradient of 20% (v/v) acetonitrile in water for 4 min, gradually rising to 80% (v/v) acetonitrile in water at 35 min. This concentration was kept constant until 40 min when the gradient was decreased to 20% (v/v) acetonitrile in water at 42 min.) Sample preparation involved mixing 20 μL of the sample with 1 mL acetonitrile-water (50:50 mixture) containing 0.1% trifluoroacetic acid. The intensity of each identified peak was determined by UV detection at 280 nm. The experimental data was acquired in triplicate and the average data was shown. The samples were vortexed before collecting the aliquots for HPLC and the percentage yields are calculated from HPLC integrated peak areas.

Transmission electron microscopy (TEM)

Transmission electron microscopy (TEM) images were captured using a LEO 912 energy filtering transmission electron microscope operating at 120kV fitted with 14 bit/2 K Proscan CCD camera. Carbon-coated copper grids (200 mesh) were glow discharged in air for 30 seconds. The support film was touched onto the gel surface for 3 seconds and blotted down using filter paper. Each sample was allowed to dry afterwards for 2-3 minutes in a dust-free environment prior to TEM imaging. Negative stain (20 μL, 1 % aqueous methylamine vanadate (Nanovan, Nanoprobes) was applied and the mixture blotted again using filter paper to remove excess. The dried grids with the samples were then imaged using the microscope.

Synthesis

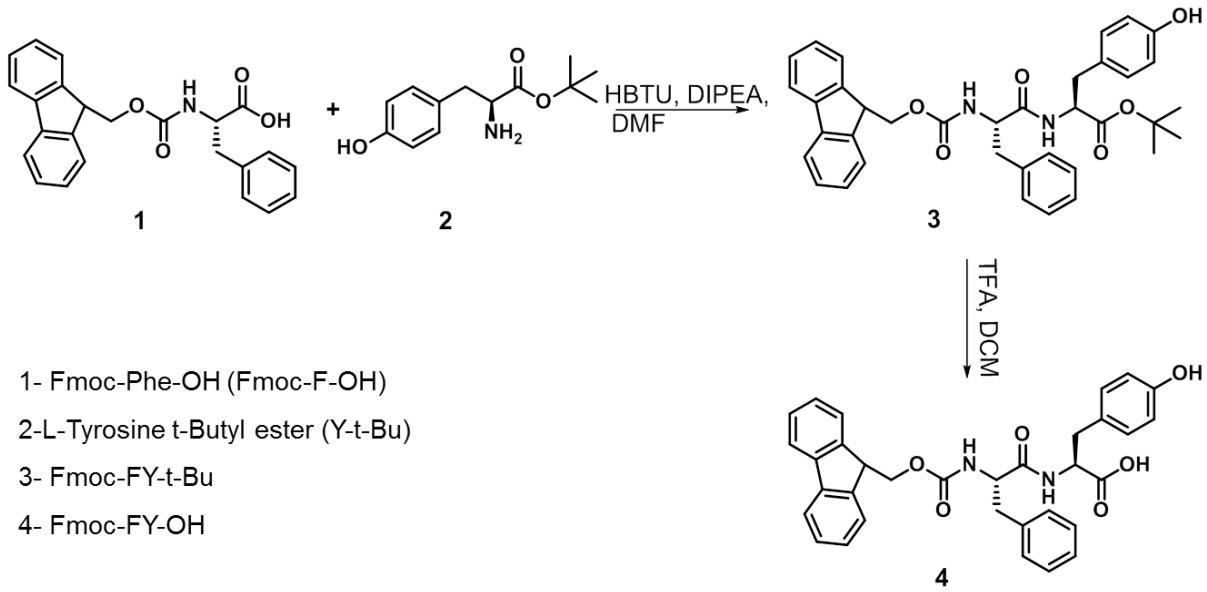

Figure S1: Reaction Scheme for chemical synthesis of Fmoc-FY-OH.

Synthesis of Fmoc-FY-t-Bu (3)

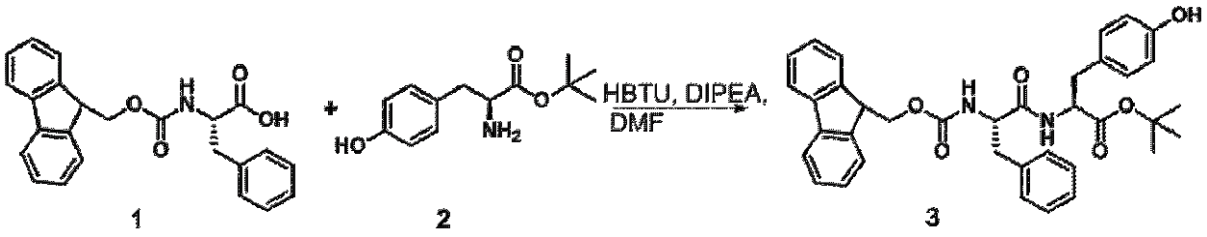

For the synthesis of Fmoc-FY-t-Bu (3), 2 g (5.16 mM) of Fmoc-Phe-OH (1) was weighed into a round bottom (RB) flask and was dissolved in 10-15 mL of DMF (dimethyl formamide), followed by addition of 1.47 g (6.2 mM) of L-tyrosine tert-butyl ester into the RB flask. 2.94 g **(7.74 mM) of** *N,N,N′,N′*-Tetramethyl-*O*-(1*H*-benzotriazol-1-yl)uranium hexafluorophosphate, *O*-(Benzotriazol-1-yl)-*N,N,N′,N′*-tetramethyluroniumhexafluorophosphate (HBTU) and 2.36 mL (12.9 mM) of Diisopropyl ethyl amine (DIPEA) was added to the reaction mixture and was stirred overnight at room temperature (RT). After the reaction was **over,** 40 mL of HPLC grade water was added to the mixture and was separated in 100 mL of ethyl acetate. The compound in organic fraction was further washed with sodium bicarbonate (NaHCO3; 60 mL), Brine (60 mL) and HCl (1N) and brine (60 mL) respectively. The organic fraction was collected and dried in anhydrous $MgSO_4$

followed by evaporating the solvent *in vacuo*. The crude product was finally purified by using column chromatography (DCM/MeOH = 98/2). The compound obtained was characterised by ^{1}H NMR and ^{13}C spectroscopy.

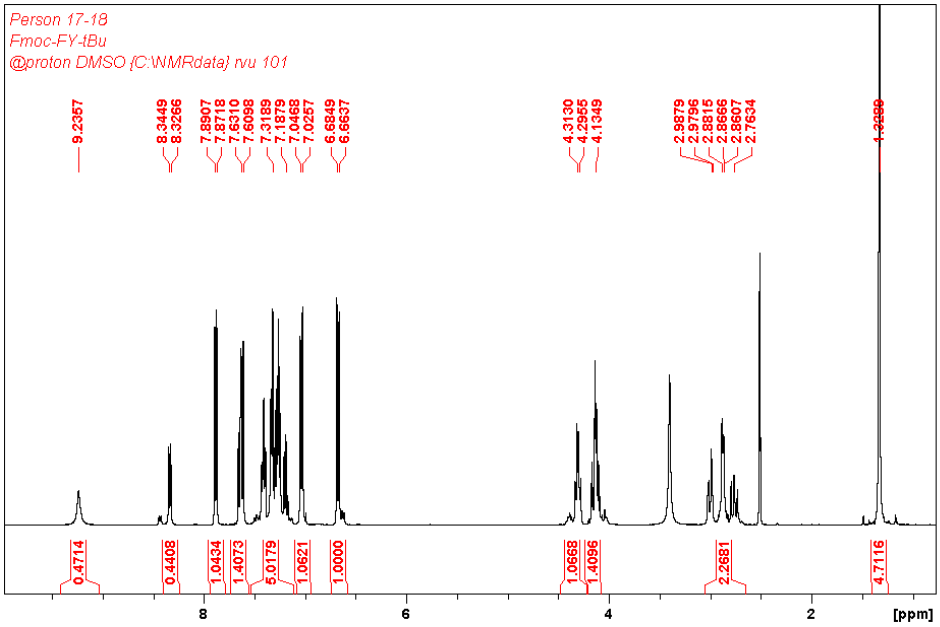

Figure S2: ^{1}H NMR of Fmoc-FY-tBu.

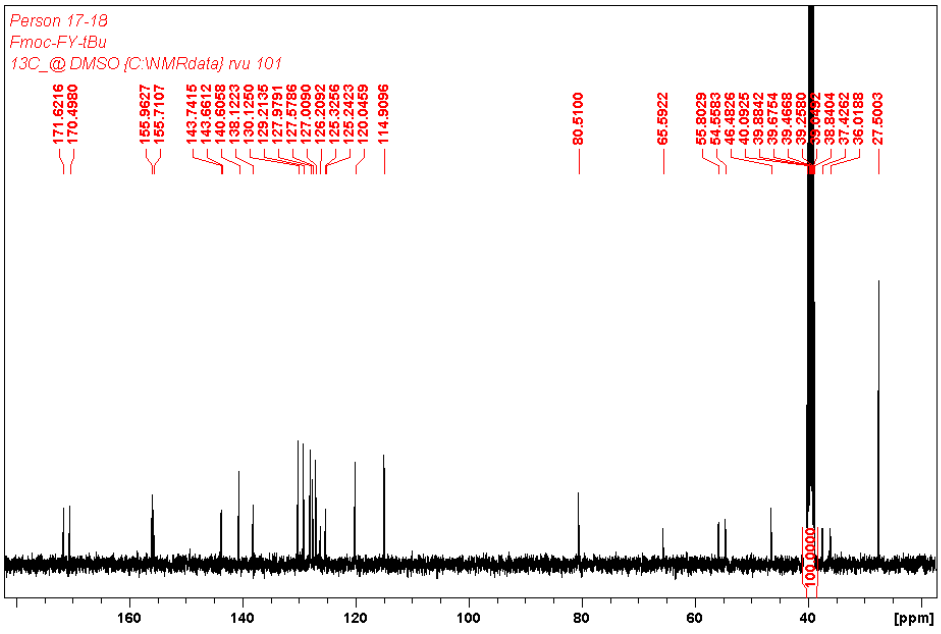

Figure S3: ^{13}C NMR of Fmoc-FY-tBu.

^{1}H NMR (DMSO-d_6, 400 MHz) δ 1.32 (S, 9H, t-Butyl), 2.86-2.98 (m, 4H, CH_2 in tyrosine and phenyl alanine moieties), 4.13 (m, 3H, CH_2 and CH- of Fmoc moiety), 4.29-4.31 (m, 2H, CH in tyrosine and phenyl alanine

moieties), 6.67 (d, 2H, CH at ortho position of OH group of tyrosine, ^{3}J = 8.4 Hz), 7.03 (d, 2H, CH at meta position of OH group of tyrosine, 3J = 8.4 Hz), 7.18-7.31 (m, 10H, Fmoc and Phenylalanine aromatic CH, CO-NH), 7.62 (m, 2H, Fmoc aromatic CH), 7.87-7.89 (m, 2H, Fmoc aromatic CH), 8.33 (d, 1H, CO-NH, ^{3}J = 7.32 Hz), 9.24 (S, 1H, OH group of Tyrosine moiety).

^{13}C NMR (DMSO d_6) 100 MHZ: 171.62 (C=O, carboxyl), 170.49 (C=O, amide), 155.96 (O-C=O, amide), 155.71 (Tyr C), 143.74, 143.66 (ArC_{Fmoc}), 140.60 (ArC_{Fmoc}), 138.12 (Phe C), 130.12 (Tyr C), 129.21 (Tyr C), 127.97, 127.57, 127.00, (Phe C), 126.20 (ArC_{Fmoc}), 125.32 (ArC_{Fmoc}), 125.24(ArC_{Fmoc}), 120.04 (ArC_{Fmoc}), 114.90 (Tyr C), 80.51 (t-Butyl C) 65.59 (CH_2), 55.80 (CH-), 54.55 (CH-), 46.49 (C_{Fmoc}-H), 37.42 (CH_2), 36.01 (CH_2) 27.50 (t-butyl CH_3).

Synthesis of Fmoc-FY-OH (4)

3 4

For the synthesis of Fmoc-FY-OH (4), 1 g of Fmoc-FY-t-Bu (3) was dissolved in 90/10 Trifluoro acetic acid (TFA)/Dichloromethane (DCM) mixture and was stirred overnight to allow the deprotection. After the reaction got over, the solvent was evapourated in vacuo followed by washing the product 3-4 times in toluene. The product obtained was characterised by ^{1}H NMR and ^{13}C spectroscopy and the purity was checked in HPLC.

^{1}H NMR (DMSO-d_6, 400 MHz) δ 2.71-3.01 (m, 4H, CH_2 in tyrosine and phenyl alanine moieties), 4.13 (m, 3H, CH_2 and CH- of Fmoc moiety), 4.38-4.41 (m, 2H, CH in tyrosine and phenyl alanine moieties), 6.66 (d, 2H, CH at ortho position of OH group of tyrosine, ^{3}J = 8.4 Hz), 7.02 (d, 2H, CH at meta position of OH group of tyrosine, 3J = 8.4 Hz), 7.25-7.30 (m, 10H, Fmoc and Phenylalanine aromatic CH, CO-NH), 7.62 (m, 2H, Fmoc aromatic CH), 7.87-7.89 (m, 2H, Fmoc aromatic CH), 8.22 (d, 1H, CO-NH, ^{3}J = 7.7 Hz), 9.22 (S, 1H, OH group of Tyrosine moiety), 12.74 (s, 1H, COOH)
^{13}C NMR (DMSO d_6, 100 MHZ)172.86 (C=O, carboxyl), 171.57 (C=O, amide), 155.92 (O-C=O, amide), 155.65 (Tyr C), 143.75, 143.64 (ArC_{Fmoc}), 140.60 (ArC_{Fmoc}), 138.12 (Phe C), 130.06 (Tyr C), 129.21 (Tyr C), 127.96, 127.58, 127.25, 127.02 (Phe C), 126.18 (ArC_{Fmoc}), 125.31 (ArC_{Fmoc}), 125.25 (ArC_{Fmoc}), 120.04 (ArC_{Fmoc}), 114.95 (Tyr C), 65.59 (CH_2), 55.92 (CH-), 53.77 (CH-), 46.49 (C_{Fmoc}-H), 37.35 (CH_2), 35.88 (CH_2)

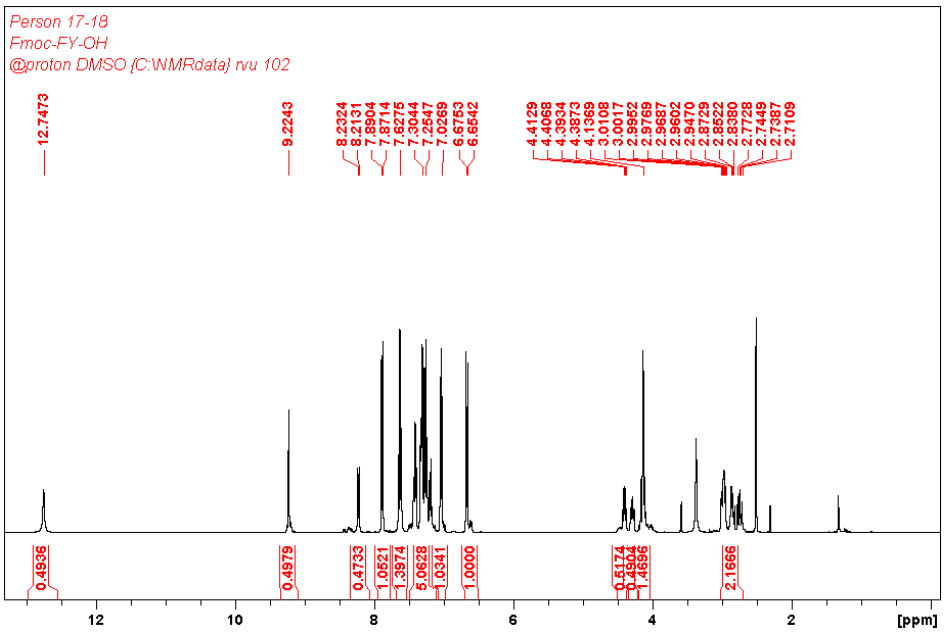

Figure S4: ^{1}H NMR of Fmoc-FY-OH.

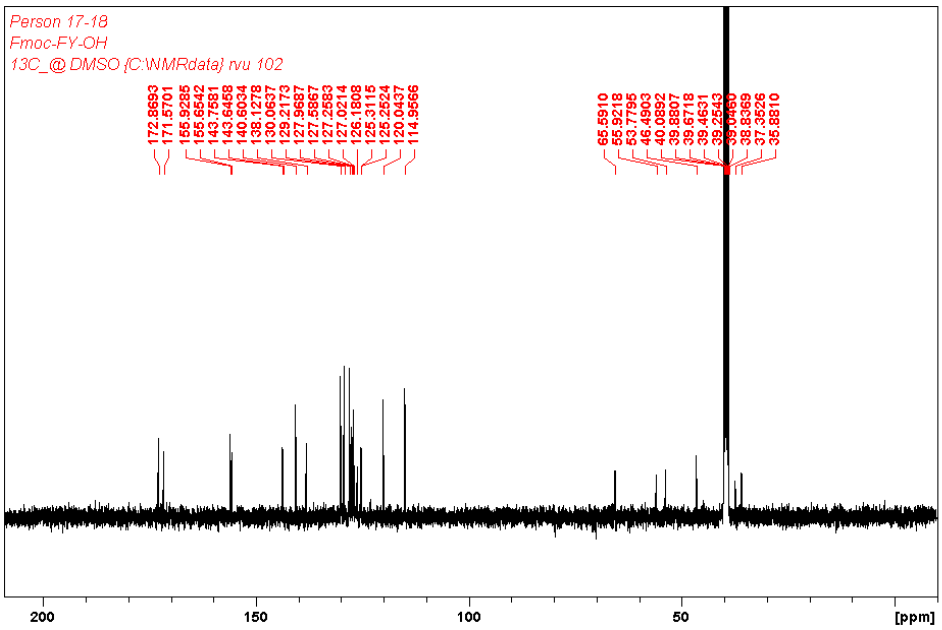

Figure S5: ^{13}C NMR of Fmoc-FY-OH.

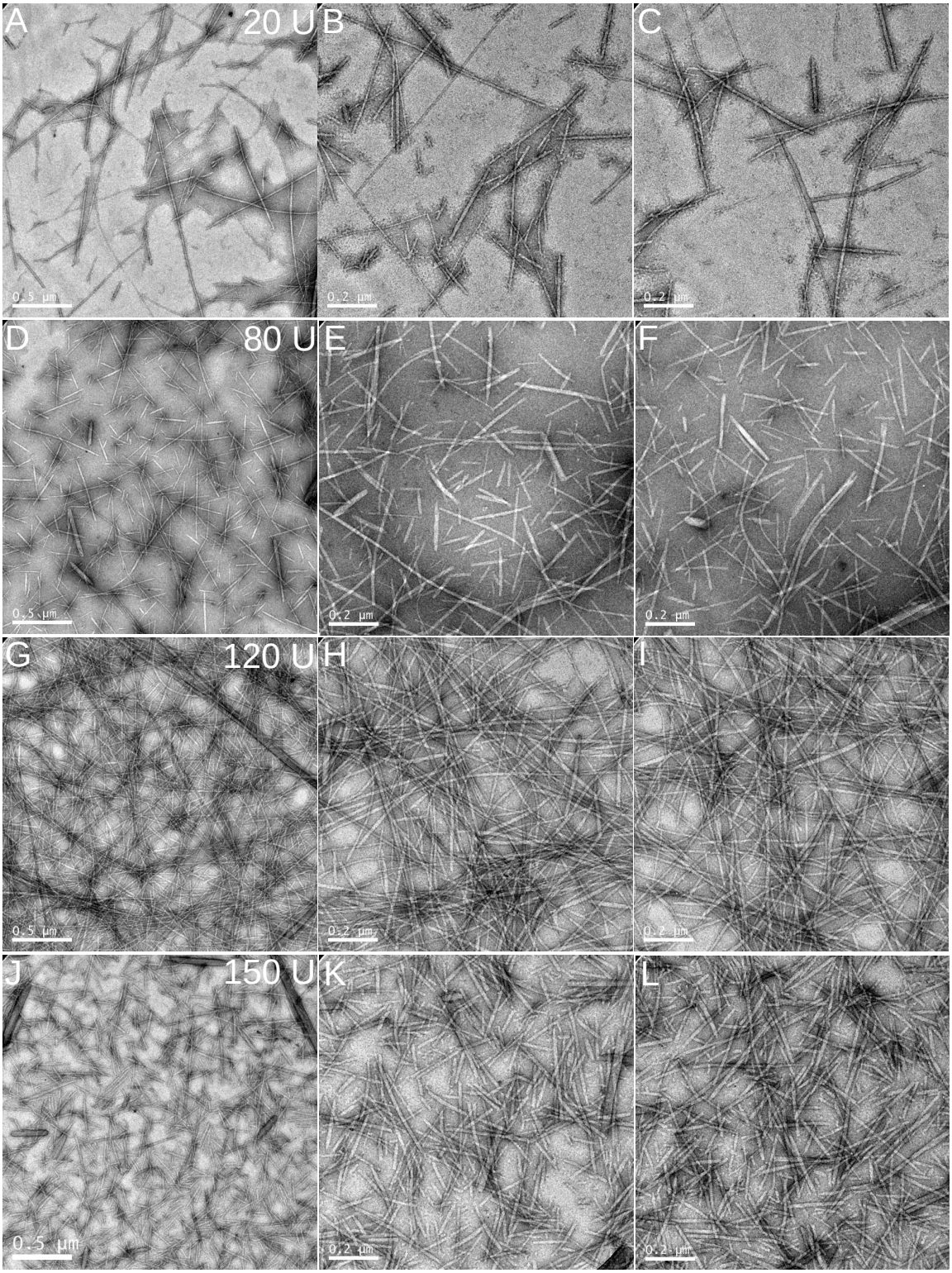

Figure S6: Transmission electron microscope data of the nanofibers at different enzyme concentrations. A, B, C) 20 U; D, E, F) 80 U; G, H, I) 120 U; J, K, L) 150 U.

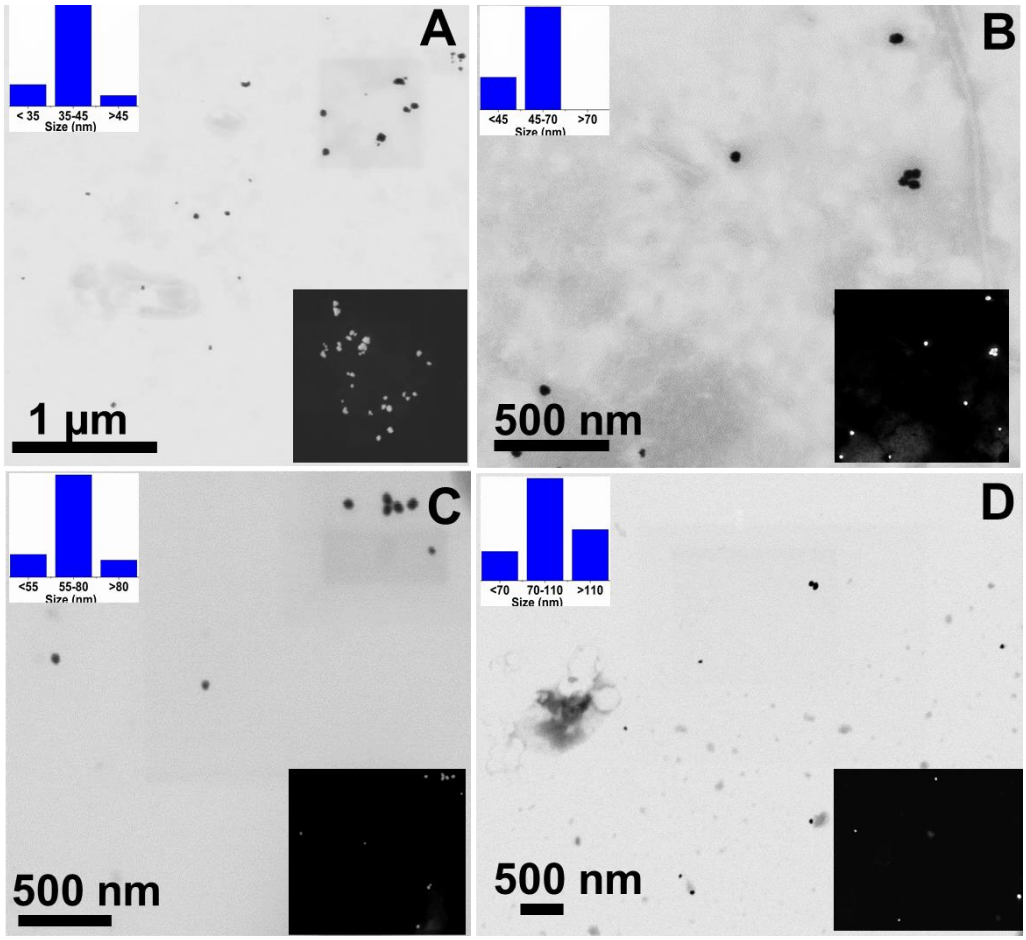

Figure S7: Transmission electron microscopy (TEM) images of gold nanoparticles formed in a hydrogel template formed at different enzyme concentration. A) 150 U/mL, B) 120 U/mL, C) 80 U/mL, D) 20 U/mL. It is observed that the concentrations of phosphatase play a key role in controlling the size of the nanoparticles generated.i.e. lower the concentration of the enzyme, larger is the nanoparticles formed and vice versa. The size of 25 nanoparticles were measured to obtain the histogram for each concentration of enzymes.

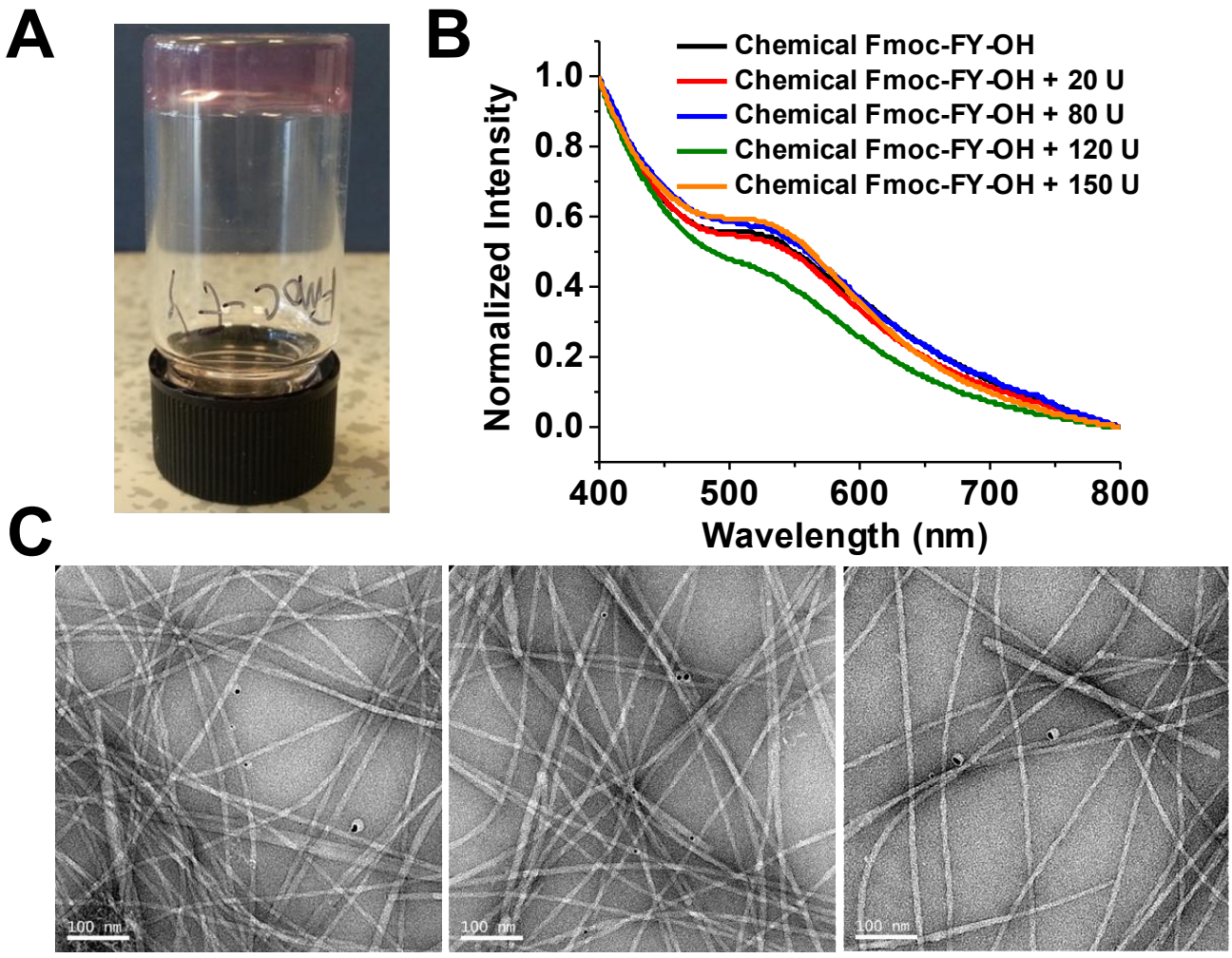

Figure S8: A) Digital image of gold nanoparticle formation in chemical hydrogel. B) UV-Vis spectra of the chemical hydrogels, followed by addition of different amount of enzyme. It was clearly noticed that, the UV-Vis spectra of nanoparticles formed in chemical gel (with addition of enzyme) do not change. C) TEM images of the nanofibers and gold nanoparticles formed for chemical Fmoc-FY-OH.

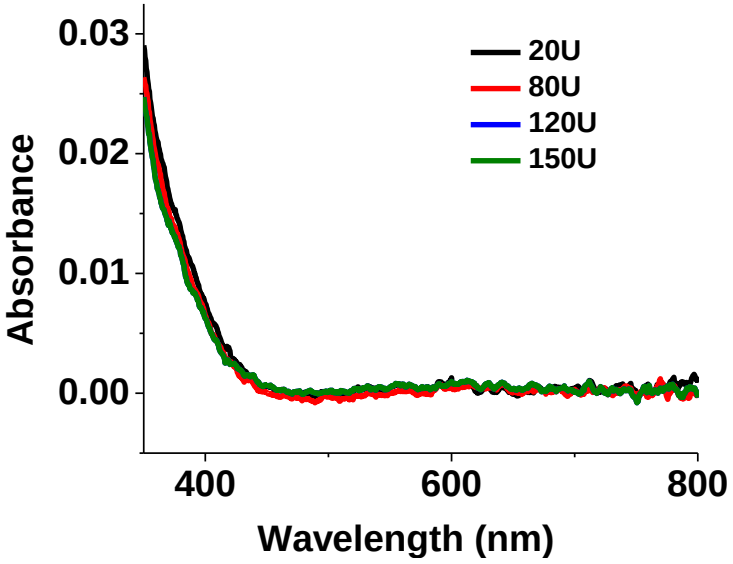

Figure S9: UV-Vis spectroscopy of reaction of phosphatase (different concentration) to gold chloride, which shows that there is no reaction of phosphatase with gold (III) chloride.

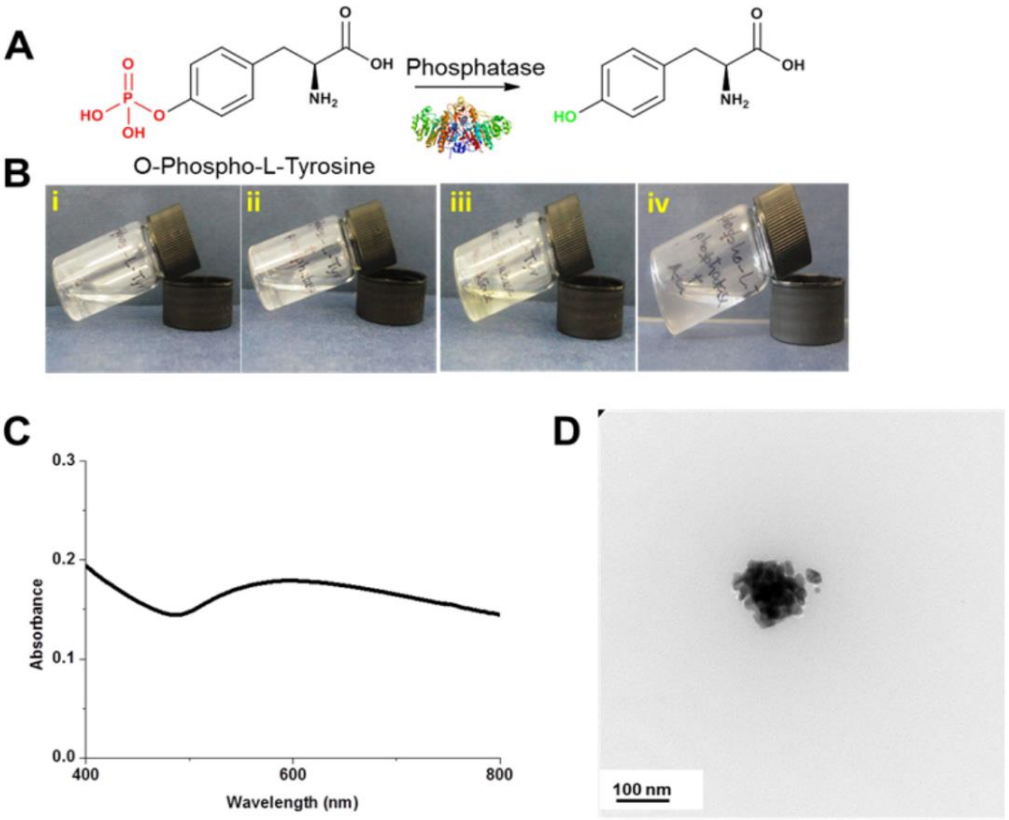

Figure S10: A) Chemical scheme for the enzymatic dephosphorylation of o-phospho-L-tyrosine. B) Digital image of enzymatic hydrolysis and gold nanoparticle formation at different stages i) o-phospho-L-tyrosine, ii) o-phospho-L-tyrosine + phosphatase, iii) o-phospho-L-tyrosine + phosphatase + Au (III) chloride solution, iv) after 24h. C) UV-vis absorption spectra of the nanoparticles formed which shows a broad peak ranging from 650-500

nm. D) TEM image of the nanoparticles formed, which are more like nanoclusters without any definite size and shape.

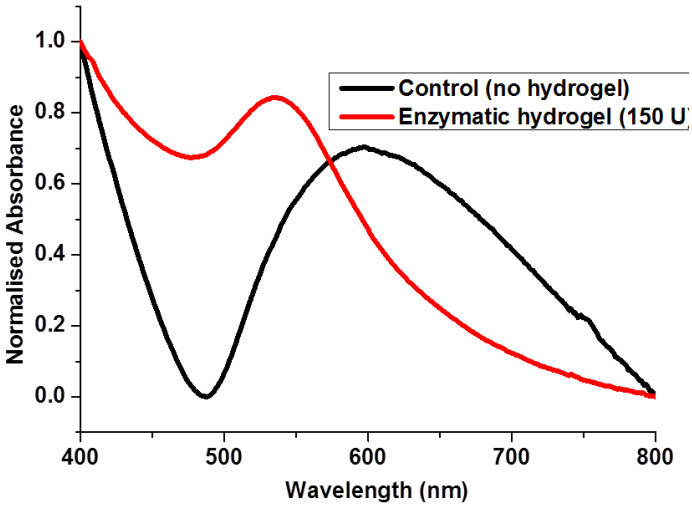

Figure S11: Monodispersity of the gold nanoparticles were enhanced in presence of a hydrogel matrix, as it is evident from the UV-vis spectroscopy. The nanofibers of the hydrogel act as stabilising agent or surfactants for the gold nanoparticles formed.

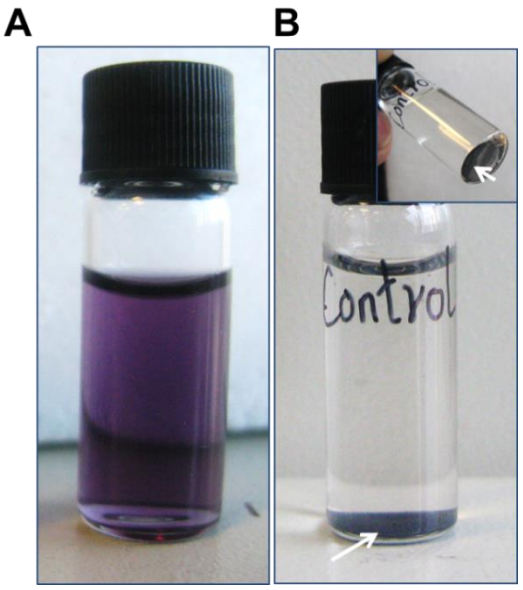

Figure S12: **Colloidal stability**: The gold nanoparticles formed in the enzymatic hydrogel template remain stable for months (A) gold nanoparticle solution synthesized in enzymatic hydrogel template (150 U), where the fibers acts as surfactant/stabilisers. (B) gold nanoparticles formed by reduction by –OH group of tyrosine (generated from hydrolysis of O-Phospho-tyrosine by phosphatase) are not stable due to absence of stabiliser and solids settle down with time as marked by arrows (inset).